Structures 44 (2022) 1070–1080

Contents lists available at ScienceDirect

Structures

journal homepage: www.elsevier.com/locate/structures

Vehicle-bridge interaction system for long-span suspension bridge under random traffic distribution

Yuefeng Shao [a,b,*], Changqing Miao [a,b,*], J.M.W. Brownjohn [c], Youliang Ding [a,b]

[a] Key Laboratory of Concrete and Prestressed Concrete Structures of Ministry of Education, Southeast University, Nanjing, PR China
[b] School of Civil Engineering, Southeast University, Nanjing 211189, PR China
[c] Vibration Engineering Section, College of Engineering, Mathematics and Physical Sciences, University of Exeter, North Park Road, EX4 4QF Exeter, United Kingdom

ARTICLE INFO

Keywords:
Random Traffic flow
Vehicle-bridge interaction
Dynamic response
Long-span suspension bridge
Monte Carlo sampling

ABSTRACT

A random traffic loading method, which is based on the actual traffic data, in vehicle-bridge interaction (VBI) system is presented in this paper. In this method, the number and type of vehicles are determined by the hourly traffic flow data. Based on the traffic flow characteristic statistics in China, the layout the traffic flow on a multi-lane road can be obtained by lane distribution probability of vehicles. After Monte Carlo sampling the vehicle gaps, the random traffic flow simulation could be carried out. By incorporating the random traffic flow into the precise time-integration based on VBI system, the dynamic response of the bridge under bridge operational load was simulated and presented here. This method has a potential feasibility for bridge's dynamic response analysis and comparison with the past structural health monitoring data. Numerical results indicate that the maximum dynamic deflection of steel girder is in the mid-span of the suspension bridge. Whereas the side-span of the suspension bridge is more sensitive to the forced vibrations excited by vehicles.

1. Introduction

As one of the most common live loads acting on a road bridge, the traffic load has a significant influence on the bridge operational safety. This dynamic load leads to the amplification effect of the static load, which mainly relate to vibrations caused by the road surface roughness and vehicle-bridge interaction (VBI) effect, which need to be accounted for in the design process [1]. With the development of dynamic theories, modelling of the VBI system had been continuously improved. Green and Cebon [2] provided the dynamic solution of a bridge, which was simplified as a Euler-Bernoulli beam, under a 'quarter-car' vehicle model. Henchi et al., [3] presented a solution of the dynamic interaction between bridge and vehicles as a the three-dimensional system. With the application of modal superposition technique and finite element method, the dynamic interaction research works [4–6] on more complex bridge models have continued.

Research developments in bridge modeling for VBI mean that the loading process can be better simulated. Zhu and Law [7] showed that the dynamic responses are larger close to the path of moving vehicle, which means the transverse vehicle position will directly affect the bridge response. Considering multi-lane bridges, Zhou et al., [8] and Zhou et al., [9] showed the differences loading effects on number of lanes, lane selection and vehicles axle configurations in vehicle-bridge interaction research. Compared to complex 3D bridge models [10], single-beam bridge models can only consider symmetrical vehicle loads, neglecting lateral load distribution.

Existing research on VBI mainly focused on the bridge characteristics [5,6,10–12] and impact of vehicle behavior [13,14]. In such research, the traffic flow design is relatively simple, generally considering the case of one vehicle crossing the bridge. Whereas for study of VBI with complex traffic flow [15,16], the type of vehicle or bridge is relatively simple. In addition, the dynamic partitioning method [17], impact coefficient analysis [18] and three-mass vehicle model analysis [19] for vehicle-bridge interaction problem are also the common research scope, but the research objects are mainly simple bridges.

To analyze the dynamic response characteristics of bridges under operating loads, the design of random traffic flow and loading methods of highway vehicle loads should be researched. Based on the vehicle types in China and the traffic flow data of Runyang bridge, a random traffic loading method was designed for VBI analysis of dynamic response of the suspension bridge. By the way, three types of multi-vehicle traffic loads were obtained by studying traffic data, while the vehicle lateral distribution was designed according to characteristic distribution of vehicles on different lanes in China. The vehicle gaps

* Corresponding authors.
E-mail addresses: 230179436@seu.edu.cn (Y. Shao), chqmiao@163.com (C. Miao).

https://doi.org/10.1016/j.istruc.2022.08.074
Received 3 May 2022; Received in revised form 15 August 2022; Accepted 16 August 2022
Available online 22 August 2022

were sampled by Monte Carlo method based on these distributions, then precise time-integration VBI [20] system was applied for the dynamic response analysis.

2. The vehicle model

2.1. The classifications of vehicle load

Based on the China General Design Specification for Highway Bridges and Culverts [21], traffic model research [22,23] and the traffic flow data provided by Runyang bridge toll station, the classifications of vehicle model could be described in terms of vehicle axle spacing, lateral tyre spacing, and the type, weight, proportion of vehicles as shown in Table 1.

The vehicle type in the traffic flow data is defined based on rules of vehicle classification used for highway tolls [24]. Then, the 13 types of vehicles in Table 1 were finally combined into five vehicle models as shown in Table 2.

2.2. The vehicle modal parameters

A three-dimensional vehicle comprised by a mass body and vehicle suspension system is shown in the Fig. 1, which takes the M5 vehicle model as an example. The mass interfaces the bridge surface through spring-dashpot systems, which consist of a suspension mass, representing the combined masses of the wheel and suspension assemblies, and the spring-dashpot of suspension and wheel, respectively. The vehicle model parameters were derived from literatures [22,23,25–27] covering vehicle modelling and relevant Chinese bridge design codes [21,24,28]. The barycenter of vehicle model was obtained by the axle weight detail and the wheelbase. These similar vehicle models are widely used in the references [6,10,12] and are considered to represent accurately vehicle-bridge interaction [27]. The parameters of M5 vehicle model in Fig. 1

Table 1
The classifications of traffic flow on Runyang Bridge.

Vehicle Label	Vehicle Type	Axles & tyres Group	Average Weight	Proportion	Lateral tyre Spacing	Axle Spacing
V1	Car	2 + 2	19kN	48.68 %	1.5 *m*	2.75 *m*
V2	Van	2 + 2	50kN	1.93 %	1.9 *m*	3.18 *m*
V3	Bus	2 + 4	115kN	4.09 %	1.9 *m*	4.2 *m*
V4	Bus	2 + 4	185kN	7.05 %	1.9 *m*	5.8 *m*
V5	Truck	2 + 2	17kN	2.41 %	1.5 *m*	2.3 *m*
V6	Truck	2 + 2	47kN	8.3 %	1.9 *m*	3.2 *m*
V7	Truck	2 + 4	98kN	4.4 %	1.9 *m*	4.3 *m*
V8	Truck	2 + 4	150kN	16.46 %	1.9 *m*	5.1 *m*
V9	Truck	2 + 4 + 4	280kN	1.04 %	1.9 *m*	4.85 m + 1.5 *m*
V10	Truck & trailer	2 + 4 + 4 + 4	370kN	0.58 %	1.9 *m*	3.6 m + 8.5 m + 1.32 *m*
V11	Truck & trailer	2 + 2 + 4 + 4 + 4	460kN	2.11 %	1.9 *m*	3.1 m + 1.5 m + 8.5 m + 1.32 *m*
V12	Truck & trailer	2 + 4 + 4 + 4 + 4	460kN	1.2 %	1.9 *m*	3.6 m + 7.26 m + 1.32 m + 1.32 *m*
V13	Truck & trailer	2 + 2 + 4 + 4 + 4 + 4	520kN	1.75 %	1.9 *m*	3.1 m + 1.5 m + 7.26 m + 1.32 m + 1.32 *m*

Note: 1. The axle spacing is the distance between adjacent axles. 2. Due to the lack of vehicle weight in the data provided by the Runyang bridge toll station, the average vehicle weights in this paper are based on the weight data in the references[22,25] of traffic flow statistics in China.

Table 2
The vehicle classification in Runyang bridge VBI system.

Vehicle Models	Axles & tyres Group	Lateral tyre Spacing	Axle Spacing	Average Weight	The Vehicle Labels included
M1	2 + 2	1.5 *m*	2.75 *m*	19kN	V1,V5
M2	2 + 2	1.9 *m*	3.2 *m*	48kN	V2,V6
M3	2 + 4	1.9 *m*	4.3 *m*	107kN	V3,V7
M4	2 + 4	1.9 *m*	5.1 *m*	160kN	V4,V8
M5	2 + 2 + 4 + 4 + 4	1.5 *m*	3.1 m + 1.5 m + 8.5 m + 1.32 *m*	440kN	V9,V10, V11,V12, V13

were explained as follows. K_{vi}, K_{ti} ($i = 1 \sim 10$) are the stiffness of the vehicle suspension and wheel respectively. C_{vi}, C_{ti} ($i = 1 \sim 10$) are the damping of the vehicle suspension and wheel respectively. M_v is the mass of vehicle body. I_p and I_r are the mass moment of inertia for pitch and rollover respectively. m_i ($i = 1 \sim 10$) are the combined masses of the suspension assemblies and vehicle wheel. a_j ($j = 1 \sim 10$) are the distance between wheel and vehicle barycenter. b_1 and b_2 are the horizontal distance between axle and vehicle barycenter. The parameters for five different vehicle models are given in Table 3-Table 5.

3. The random traffic flow distribution based on actual traffic conditions

3.1. Traffic volume analysis based on Daily traffic flow of Runyang bridge

The traffic volume detail in the random traffic flow design was obtained from the hourly traffic flow data of Runyang bridge in 2009, which provided by Runyang bridge toll station, classified based on Table 2. According to this data from December 3rd to December 9th in 2009, it was found that the hourly traffic volume of every vehicle type shows a regular distribution. Taking the hourly traffic data on December 3rd as an example (as shown in Fig. 2), each bar represents the traffic volume of one vehicle type in one hour, and the curve represents the total volume of traffic flow in one hour. The volume variations of M1, M2 and M3 vehicles were similar, and the traffic density of these vehicles was relatively high between 7:00 to 22:00 during a day. The M1 vehicles were most common in the daytime, and the largest hourly traffic volume in a day exceeded 2000. For the heavy vehicles, such as M4 and M5, their high traffic densities are mainly concentrated between 0:00 to 5:00 and 16:00 to 24:00. Since the traffic flow changed regularly with time, hourly traffic volume was used in traffic distribution design. Three typical hourly traffic volumes, which were the average traffic volume during the day, the largest total traffic volume (during 16:00 to 17:00) and the largest traffic volume of heavy vehicles (during 22:00 to 23:00), were selected as the loading cases in VBI dynamic response analysis. Three typical traffic volumes were selected as shown in Table 6. The traffic volumes at 16:00–17:00 is the largest, but the vehicle M1 accounted for about two-thirds, while the heavy vehicle (M4 and M5 vehicle models) volumes at 22:00–23:00 increased significantly compared to 16:00–17:00.

3.2. Plane distribution analysis of random traffic flow

Runyang suspension bridge is a two-way six-lane bridge (as shown in Fig. 3). The design of random traffic flow should mainly focus on the lane selection and the vehicle gaps. The overtaking and lane changing of vehicles are ignored in random traffic flow design because of the low traffic density. Based on the traffic volume statistics at the entrance and exit of the bridge toll station, the proportion of two-way traffic flow is obtained as shown in the Fig. 4.

As shown in Fig. 4, it could be found that the proportion of traffic volume at the entrance and exit is almost equal. Therefore, it was assumed that traffic volume of the bridge was the same in both

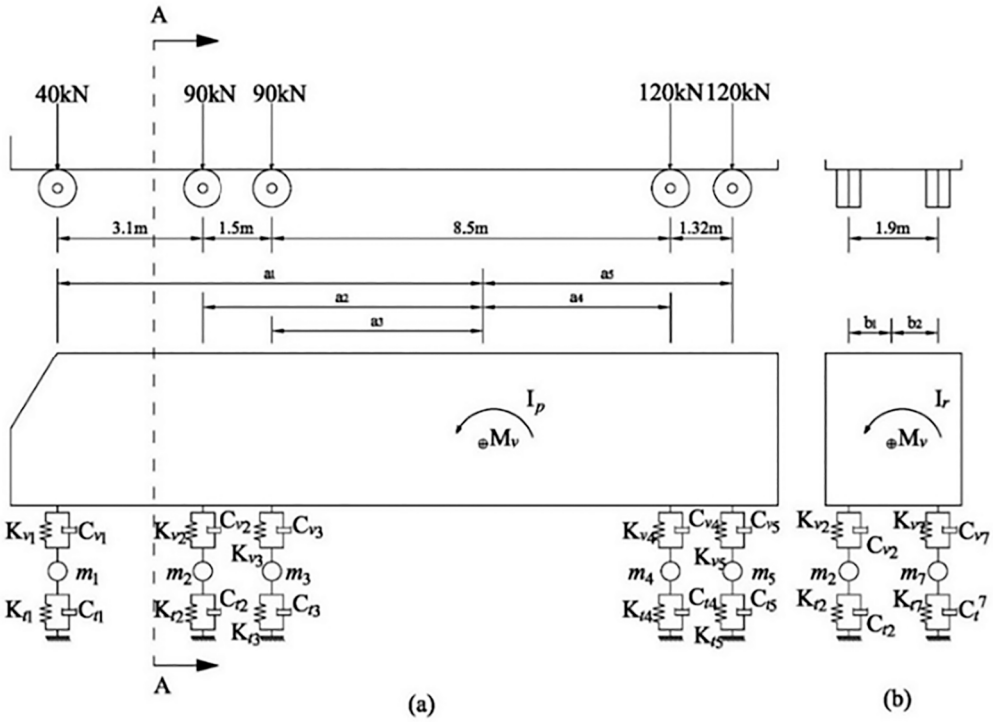

Fig. 1. M5 vehicle model sketch (13-degree of freedoms), (a) side view, (b) section A-A.

Table 3
the parameter of proposed Chinese vehicle models.

Vehicle Model	Vehicle body mass (kg)	Pitch moment of inertia (kg·m^2)	rollover moment of inertia (kg·m^2)	Axle	Mass of suspension assemblies & tyre
M1	1139	2122.2	641	Front	200
				Rear	200
M2	3327	5656	1291	Front	340
				Rear	445
M3	8559	15,406	2825	Front	500
				Rear	680
M4	13,327	28,845	3598	Front	700
				Rear	800
M5	36,300	229,444	35,235	Front	700
				Middle	1000
				Rear	800

Note: The middle axle mass of suspension assemblies & tyre including m_2, m_3, m_7 and m_8. The rear axle mass of suspension assemblies & tyre including m_4, m_5, m_9 and m_{10}.

Table 4
Geometric parameters of proposed Chinese vehicle models.

Vehicle Model	parameter	Value (m)	parameter	Value (m)
M1	a_1	1.447	b_1	0.75
	a_2	1.303	b_2	0.75
M2	a_1	1.867	b_1	0.95
	a_2	1.333	b_2	0.95
M3	a_1	2.693	b_1	0.95
	a_2	1.607	b_2	0.95
M4	a_1	2.550	b_1	0.95
	a_2	2.550	b_2	0.95
M5	a_1	8.15	b_1	0.95
	a_2	5.05		
	a_3	3.55	b_2	0.95
	a_4	4.95		
	a_5	6.25		

Table 5
Stiffnesses and damping of the proposed Chinese vehicle model.

vehicle parameter	Front axles	Middle axles	Rear axles	Front tyre	Middle tyre	Rear tyre
M1 stiffness (kN·m^{-1})	251.9	–	251.9	240	–	240
M2 stiffness (kN·m^{-1})	300	–	350	500	–	500
M3 stiffness (kN·m^{-1})	300	–	500	500	–	500
M4 stiffness (kN·m^{-1})	350	–	650	500	–	750
M5 stiffness (kN·m^{-1})	400	1000	750	1750	3500	3500
M1 damping (kN·s·m^{-1})	3	–	3	2	–	2
M2 damping (kN·s·m^{-1})	3	–	3	3	–	3
M3 damping (kN·s·m^{-1})	3	–	3	3	–	3
M4 damping (kN·s·m^{-1})	5	–	5	5	–	5
M5 damping (kN·s·m^{-1})	10	10	10	10	0	0

directions. Then, based on the investigation about the vehicle distribution characteristics in China [8,9,29] and the traffic volume assumption in two-way directions, a three-lane road model was selected in the vehicle lanes distribution analysis. The probability of lanes selection for different vehicle types based on the three-lane traffic model in China is shown in Fig. 5.

Based on the lane division of Runyang bridge, the statistics of lane selection characteristics of different vehicle models have the following characteristics:

1. M1 vehicles, which account for the most part of traffic volume, mainly drove in the inner two lanes.
2. M2 vehicles were mainly driven in the two outer lanes.
3. The midsize vehicles M3 and heavy vehicles M4, M5 preferred to

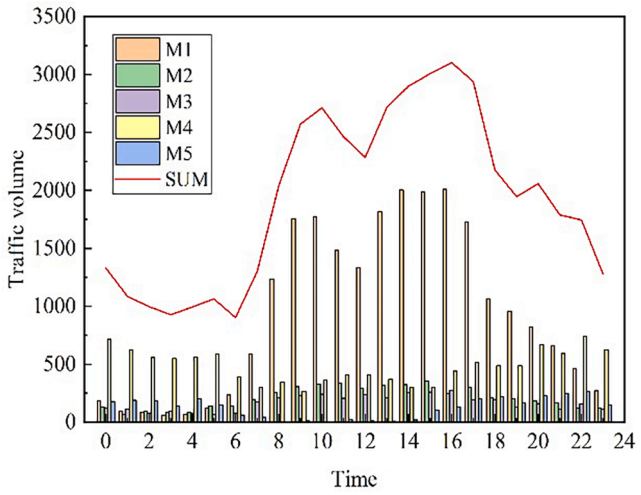

Fig. 2. Hourly traffic volume detail on Dec 3rd in 2009.

Table 6
Three typical traffic volumes of vehicles.

Vehicle Model	Traffic Volumes at 16:00–17:00 (Case1)	Traffic Volumes at 22:00–23:00 (Case2)	Average Daily Traffic Volumes (Case3)
M1	2031	404	988
M2	278	128	198
M3	248	115	164
M4	393	582	455
M5	86	207	129
SUM	3036	1256	1934

drive in the outermost lane rather than driven in the middle lane, and almost none of these vehicles were driven in the innermost lane.

The lane selection significantly affects the traffic flow composition of every lane, which in return affects the lanes loads and their load responses [9].

Another key factor of random traffic flow design is the vehicles gap. The stochastic process model researches of vehicle loads [23,30] and the traffic distribution surveys in China [31] show that vehicle gap probability distribution could be described by lognormal distribution or Weibull distribution. Due to lack the vehicle gap survey of Runyang Bridge, the vehicle gap data for highway bridges in Jiangsu province [31,32], where Runyang Bridge is located, was referred in this distribution analysis of random traffic flow. Based on the vehicle gap probability distribution of Xinyi River Bridge, the lognormal distribution (as shown in Eq.(1)) was chosen to describe the vehicle gap.

$$f(x) = \frac{1}{\sqrt{2\pi}\sigma x}\exp[-\frac{(\ln x - \mu)^2}{2\sigma^2}] \quad (1)$$

By fitting the vehicle gap probability distribution on different lanes of the highway bridge in Jiangsu province, the parameters of the lognormal distribution were estimated as:$\widehat{\mu} = 4.929446, \widehat{\sigma} = 0.985583$.

3.3. The generation process of random traffic flow

The random traffic flow needs to satisfy the following assumptions:

1. In vehicle models, constant vehicle speed, wheel-bridge contact at one single point, vertical vehicle forces and linear stiffness and damping elements are assumed.
2. In good traffic condition, no traffic jams.
3. Vehicles do not change lanes and overtake others.

In addition, it takes about 54 s to pass the Runyang Bridge at the speed of 100 km/h. After considering the continuity of the traffic flow

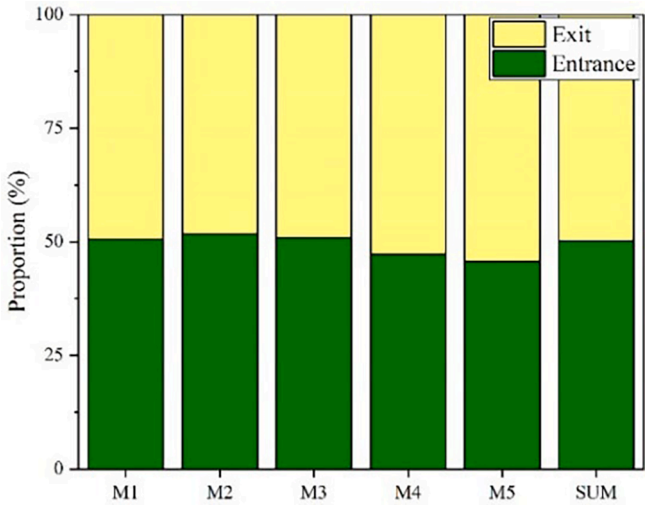

Fig. 4. The proportion of traffic volume at the entrance and exit of the Runyang bridge toll station.

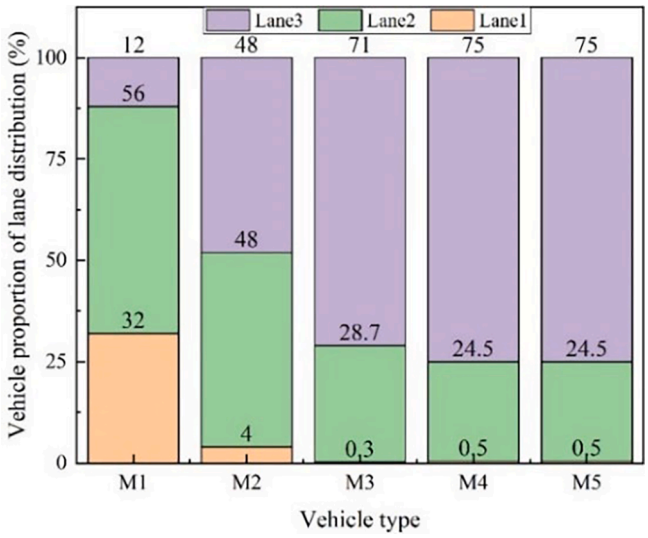

Fig. 5. Vehicles distribution proportion on different lanes.

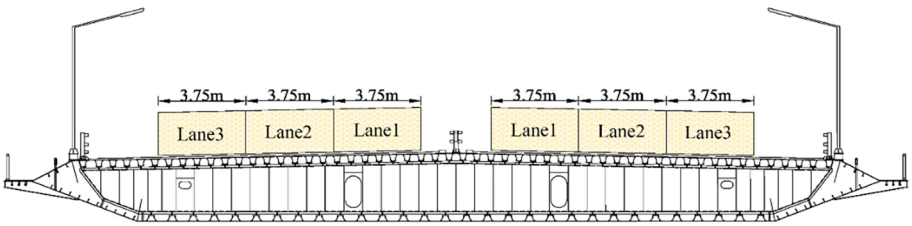

Fig. 3. Lane division cross section of Runyang suspension bridge.

and the computational effort in VBI system, 5 min, which is 5 times as long as the vehicle was driven cross the bridge, was determined as the traffic flow loading time. Based on this loading time and the traffic density, the traffic volumes for different vehicle models in three loading cases are shown in Table 7.

After determining the traffic volume for each loading case, the selection of lanes, the sequence of vehicles entering the bridge and the distance between vehicles are randomly sampled by Matlab to generate the random traffic flow. The generation process is shown in Fig. 6.

4. The introduction of Runyang bridge and VBI system

4.1. The finite element model and modal parameters of Runyang suspension bridge

The Runyang bridge system, which was opened to traffic in 2005, crosses the Yangtze River and connects the two cities of Yangzhou and Zhenjiang in Jiangsu Province. This bridge system is composed of one suspension bridge and one cable-stayed bridge. The Runyang suspension bridge is a double tower and three-span steel box girder bridge with the span layout of 470 m + 1490 m + 470 m [33]. The width and height of the streamlined steel box girder are 36.3 m and 3.0 m respectively. The configuration of Runyang suspension bridge is shown in Fig. 7.

As shown in the cross section of the box girder, the thickness and spacing of each part of the main girder is as follows: The thickness is 14 mm at the box girder roof, 12 mm at girder edge plate, 10 mm at the box girder bottom plate, and 6 mm at U-shaped stiffener plate. The widths of the U-shaped stiffeners located at the girder roof are 300 mm at the top and 169.3 mm at the bottom. The height is 280 mm, and there are spaced at 600 mm centers. The wide of U-shaped stiffeners, which located at bottom of the girder, are 180 mm at the top and 400 mm at the bottom. The height is 250 mm, and their spacing is 900 mm. The thickness of the box girder diaphragm is 10 mm, and their spacing is 3.22 m. The elasticity modulus of steel and is $2.1*10^5$MPa.

The concrete elastic modulus of the bridge tower is $3.45*10^4$MPa. The tower height is 207.58 m, and the tower beams are set at the heights of 41.45 m, 141.3 m and 197.58 m respectively. The section size of the column decreases from bottom of the tower to top. Since this study concentrated on the vehicle-bridge interaction response of the main girder, the bridge tower cross size is simplified to three different sections in the analysis. The detail of tower parameters is shown in the Table 8. And the parameters of main cable and suspenders are shown in Table 9.

The finite element model of Runyang suspension bridge was built in ANSYS. The main girder of bridge, bridge tower, main cable and suspenders were modeled by SHELL63, BEAM4, and LINK10 elements respectively. To perform the vehicle-bridge interaction analysis, the modal parameters of the bridge are required. For comparing the difference between the finite element bridge model and the actual structure, the first eight vibration modes obtained by simulation and measurement [33,34] are presented in the Table 10. The frequencies are well matched.

4.2. The description of VBI system and road surface roughness

Based on the vehicle-bridge interaction system [35] proposed by the author and since response would remain in the linear range, modal superposition was applied to reduce the computation in the vehicle-bridge dynamic analysis. The modal parameters, such as mass, stiffness and damping, could be obtained from the unity scaled vertical mode shapes of structure, and the vehicle motion equation of the bridge and vehicle are shown in the Eq.(2)-Eq.(3).

$$\frac{1}{DMX_r^2}\left[\left\{\ddot{\xi}_b\right\}+\left(\alpha+\beta\overline{\omega}_r^2\right)\left\{\dot{\xi}_b\right\}+\overline{\omega}_r^2\{\xi_b\}\right]=\left[\phi_{i,r}\right]^T\{F_b\} \tag{2}$$

$$[M_v]\cdot\left\{\ddot{d}_v\right\}+[C_v]\cdot\left\{\dot{d}_v\right\}+[K_v]\cdot\{d_v\}=-\{F_G\}+\{F_{v-b}\} \tag{3}$$

where $\left\{\ddot{\xi}_b\right\},\left\{\dot{\xi}_b\right\},\{\xi_b\}$ are the bridge normal coordinates corresponding acceleration, velocity and displacement vector; $\{F_b\}$ is forces vector of the bridge; α and β are the Rayleigh damping coefficients; $\overline{\omega}_r$ is the mode frequency of structure; $\{\phi_{i,r}\}$ is r^{th} unity scaling mode shape of the bridge at node i; DMX_r is the maximum value of normalized mode shape;$[M_v],[C_v],[K_v]$ are the vehicle structural matrices of mass, damping and stiffness, respectively; $\left\{\ddot{d}_v\right\}$, $\left\{\dot{d}_v\right\}$, $\{d_v\}$ are the vertical acceleration, velocity and displacement vector of vehicle model; $\{F_G\}$ is the gravity load of vehicle; $\{F_{v\text{-}b}\}$ is the interaction force between the bridge and vehicle..

When a vehicle is present on the bridge, the interaction force between j^{th} wheel and bridge is:

$$F_{v-b}^j=-F_{b-v}^j=-K_{tj}\cdot\Delta_j-C_{tj}\cdot\dot{\Delta}_j\quad(j=1,2,3\ldots) \tag{4}$$

$$\Delta_j=d_{tj}-d_{b\_contactj}-r_j(x),\quad \dot{\Delta}_j=\dot{d}_{tj}-\dot{d}_{b\_contactj}-\dot{r}_j(x) \tag{5}$$

where F_{v-b}^j and F_{b-v}^j are the vehicl loads acting on the bridge and bridge reaction loads acting on the vehicle respectively; Δ_j and $\dot{\Delta}_j$ are the relative vertical displacement and velocity between the jth wheels and bridge respectively; K_{tj} and C_{tj} are the stiffness and damping of wheels; d_{tj} and $\dot{d}_{tj}$ are the vertical displacement and velocity of jth wheel; $d_{b\_contactj}$ and $\dot{d}_{b\_contactj}$ are vertical displacement and velocity of bridge at jth wheel; $r_j(x)$ road surface roughness under jth wheels.

In FE structure dynamic analysis, $d_{b\_contact}$ could be obtained by using the bridge shape function equation, which is based on the interaction load between jth vehicle wheels and bridge, and the bridge finite element structure node displacement.

$$d_{b\_contactj}=\left[N_b^j\right]\cdot\{d_b\} \tag{6}$$

where $\left[N_b^j\right]$ is the bridge shape function under jth wheel; $\{d_b\}$ is the equivalent node displacement of bridge finite element model.

Based on the modal correlation factor [35], the first 50 modes related to deck vibration participate in the VBI operation, which have a good performance in VBI simulation.

Since the traffic data in this analysis was three years after the bridge opened to traffic, the degree of the road surface roughness is assumed as grade A, based on the relevant code [36] in China. The distribution of the road surface roughness can be represented by a periodic modulated random process [37]. The road surface roughness function d(x) in the time domain can be simulated by the spectral representation method for the displacement power spectral density (PSD) of the road surface roughness$G_d(f_i)$, which is given in the code [36] via Eq.(7) [3].

$$d(x)=\sum_{i=1}^{N}\sqrt{4G_d(f_i)\Delta f}\cos(2\pi f_i x+\theta_i) \tag{7}$$

where f_i is the spatial frequency, Δf is the spatial frequency distance interval between successive ordinates of the surface profile, and θ_i is a set of independent random phase angle uniformly distributed between 0 and2π. Then the road surface roughness can be obtained such as shown

Table 7
Traffic volume of different vehicles whin load time.

Vehicle Model	Case1	Case2	Case3
M1	170	34	83
M2	24	11	17
M3	21	10	14
M4	33	49	38
M5	8	18	11

Note: Data is rounded up.

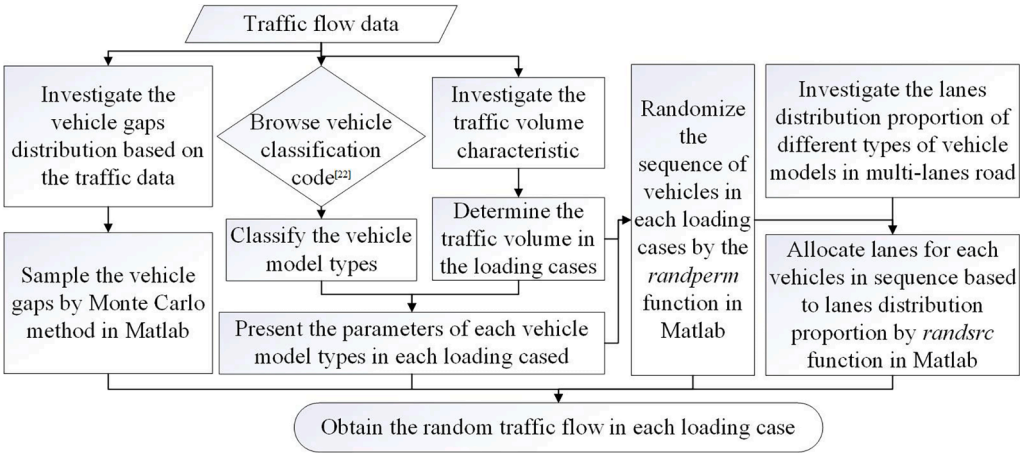

Fig. 6. The flow chart of random traffic flow generation.

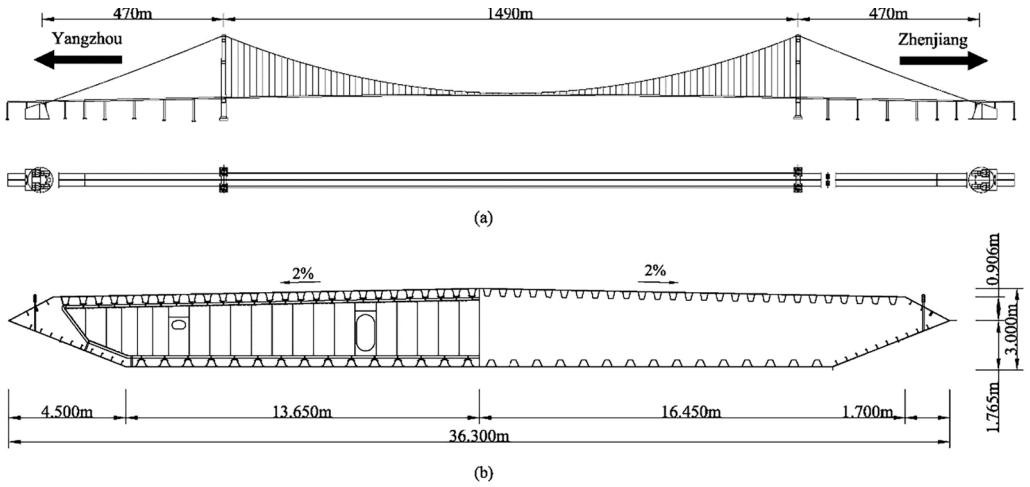

Fig. 7. Configuration of Runyang suspension bridge: (a) bridge schematic; (b) cross section of steel box girder.

Table 8
The tower parameters detail of Runyang suspension bridge.

Structural component	Area (m^2)	Bending moment of inertia I_z (m^4)	Bending moment of inertia I_y (m^4)	Anti-torsional moment of inertia I_x (m^4)
Upper column	28.7835	145.9248	371.5682	305.3238
Middle column	36.2809	172.2066	570.0485	399.2019
Bottom column	65.1729	224.4254	932.1290	487.2490
Upper beam	24.0640	243.8944	214.8489	338.9762
Middle beam	25.3920	306.2156	232.1306	392.8676
Bottom beam	34.2880	589.6408	469.7628	772.3233

Table 9
main cable and suspenders parameters of Runyang suspension bridge.

Structural component	Parameters	Value
Main Cable	Area (m^2)	0.5155
	Elasticity modulus (MPa)	$2.0*10^5$
	Density (kg/m^3)	$7.86*10^3$
Suspenders	Area (m^2)	$4.28*10^{-3}$
	Elasticity modulus (MPa)	$2.0*10^5$
	Density (kg/m^3)	$7.21*10^3$

in Fig. 8.

5. Result

5.1. The dynamic response of Runyang bridge

Based on the analysis of vehicle-bridge interaction, the dynamic response of bridge was obtained. To verify the bridge response, the maximum acceleration at the measuring point of Runyang bridge was compared with response of the bridge recorded by the structural health monitoring (SHM) data, which is shown in the Fig. 9. Based on the modal analysis of Runyang bridge [38], the first 40 modes frequencies of Runyang bridge are within 1 Hz. Since the SHM data contain signal noise, the SHM data was low pass filtered with the threshold of 1 Hz.

As shown in Fig. 9, the maximum acceleration from the SHM data is slightly larger than that obtained from the VBI system simulation. However, the three cases have similar maximum acceleration variation along the bridge direction. The maximum value of acceleration is simulated for the 1/8-span position while the acceleration at 1/2-span is relatively smaller compared to other spanwise location. The values at 1/4-span and 3/8-span are similar. Thus, the dynamic responses of Runyang bridge obtained by the VBI system have reference value compared with the actual cases.

The displacement time histories at 1/2-span for three cases are shown in Fig. 10 with the maximum displacement of Runyang suspension bridge under the action of traffic load being 0.28 m. In Case1, the

Table 10
Vibration modes and natural frequencies of Runyang suspension bridge.

Order	Mode shape	Calculated frequency (Hz)	Measured frequency (Hz)
LS1	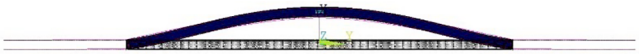	0.0606	0.0634
	1st symmetric lateral bending		
VS1	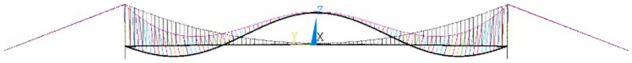	0.1254	0.1227
	1st symmetric vertical bending		
VA1	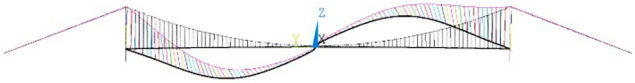	0.1439	0.1440
	1st asymmetric vertical bending		
LA2	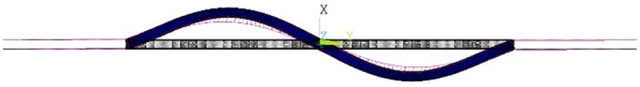	0.1516	–
	1st asymmetric lateral bending		
VS2	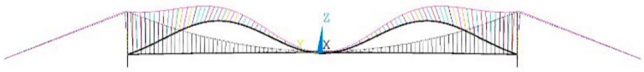	0.1667	0.1635
	2nd symmetric vertical bending		
VA2	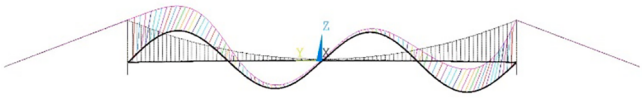	0.1888	0.1892
	2nd asymmetric vertical bending		
VS3	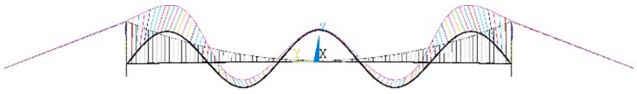	0.2414	–
	3rd symmetric vertical bending		
TS1	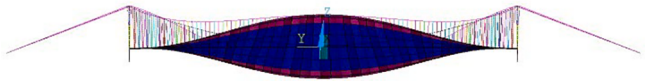	0.2648	0.2423
	1st symmetric torsion		

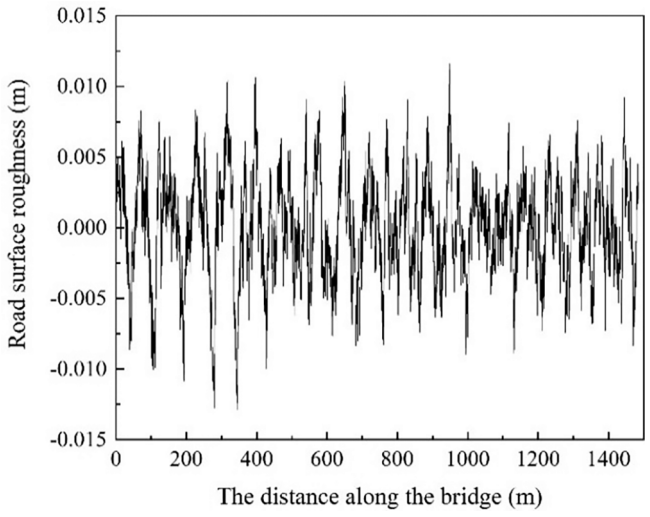

Fig. 8. The road surface roughness of Runyang bridge.

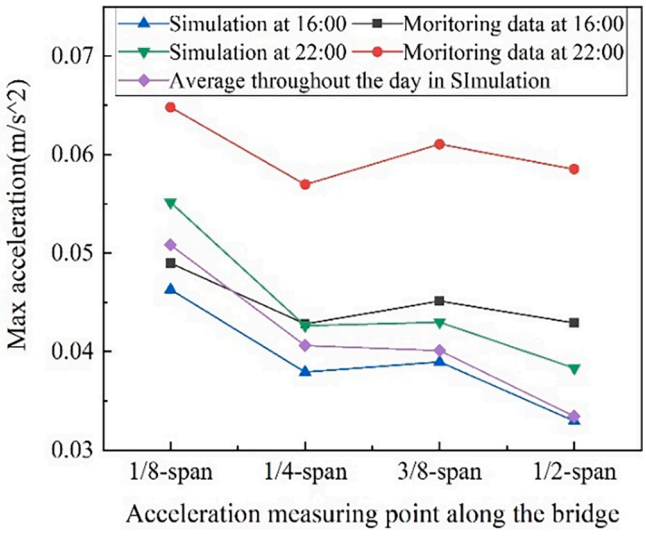

Fig. 9. The comparation of max acceleration between simulation and SHM data.

number of vehicles is the largest, but the maximum displacement only occurs when the heavy vehicles, such as M4 and M5 vehicle are on the bridge. The total number of vehicles is the least, but the number of heavy vehicles is the largest in Case2. In this Case, the bridge displacement fluctuation is the most severe. The bridge displacement in Case3 is between the first two. Comparing the displacement time histories in the three cases, the bridge displacement is more sensitive to the volume of heavy vehicles rather than other factors, such as the volume of total traffic flow. Thus, the displacement responses at the key points of the

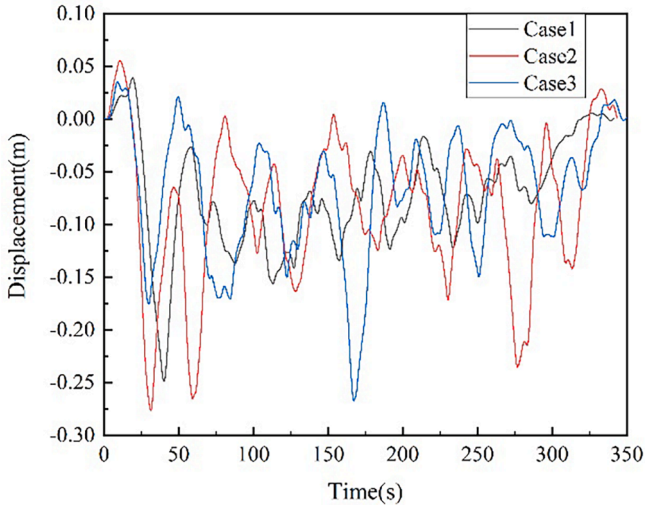

Fig. 10. The displacement time histories of 1/2-span in three cases.

bridge in Case2 are shown in Fig. 11.

For the displacement response of Case2, the maximum displacement occurs at the 1/2-span of the bridge. However, the maximum displacement at 3/8-span is also significant. To compare the displacement at different bridge locations in different loading cases, the maximum displacements at different bridge locations for three loading cases are presented in Table 11. And the displacement values are 'unity scaled' by the maximum displacement at 1/2 span in Case3. As shown in Table 11, it can be found that the maximum displacement at 3/8-span of bridge is close to that at the 1/2-span of bridge in three loading cases, especially in Case2, which has the largest number of heavy vehicles. What more, the displacement at 1/4 span of the bridge is affected by the traffic density and the volume of heavy vehicles at the same time. Because there is highest traffic density in Case1, and there is largest volume of heavy vehicle in Case2.

5.2. Vibration frequency analysis

Based on the dynamic response analysis, the case2, which has the largest displacement response, was selected for the vibration frequency analysis. According to modal analysis of Runyang suspension bridge models [38], the frequency band within 0 Hz to 1 Hz was selected in the bridge natural frequency analysis.

Since the load cases are all obtained by random sampling, the acceleration time history is satisfied the ergodic assumption. The power spectral densities (PSD) of acceleration within bridge's natural frequency at 1/8-span, 1/4-span, 3/8-span and 1/2-span of Runyang suspension bridge are shown as Fig. 12 to Fig. 15 respectively.

As shown in Fig. 12 to Fig. 15, the vibration frequency of Runyang suspension bridge in VBI analysis is mainly concentrated between 0 Hz and 0.5 Hz. Comparing the acceleration PSD distribution at different locations of bridge, it can be found that the vibration at the side span of bridge is more affected by the high modes, whose frequency are within 0.2 Hz to 0.5 Hz. However, the influence of low modes on bridge vibration increases when the location is close to 1/2-span. In the PSD distribution at 1/2-span, the modes frequencies of VS1, VS2, VA2, VS3 can be clearly identified from the amplitude peak of acceleration PSD.

Since VBI process is a forced vibration of bridge excited by vehicles. The excited frequencies of vehicles are mainly comprised by vehicle body-bounce frequencies and vehicle axle-hop frequencies, which are always distributed between 2 Hz and 5 Hz and 10 Hz to 15 Hz respectively. Thus, the acceleration PSD distribution between 1.5 Hz and 16 Hz at 1/8-span, 1/4-span, 3/8-span and 1/2-span of Runyang suspension bridge are shown as Fig. 16 to Fig. 19 respectively.

In the Case2, the vehicles' body-bounce frequencies and axle-hop frequencies are mainly between 2 Hz and 3.5 Hz and 8 Hz to 14 Hz respectively. Comparing the Fig. 16 to Fig. 19, it can be found that the PSD amplitude excited by axle-hop at different locations of bridge are similar, however the fluctuation of PSD amplitudes excited by vehicles' body-bounce at different locations is significant. The amplitude of PSD excited by vehicles' body-bounce decreases gradually from 1/8-span to 1/2-span of the bridge, which means the bridge forced vibration caused by the vehicle body-bounce have obvious regional sensitivity. Such forced vibration has much greater influence on side-span of bridge more than on the mid-span of the bridge.

Table 11
Maximum displacement proportion at different bridge locations for three loading cases.

	1/8-span	1/4-span	3/8-span	1/2-span
Case1	0.6005	0.8263	0.7717	0.9495
Case2	0.6776	0.8728	0.9911	1.0784
Case3	0.6525	0.6561	0.8450	1

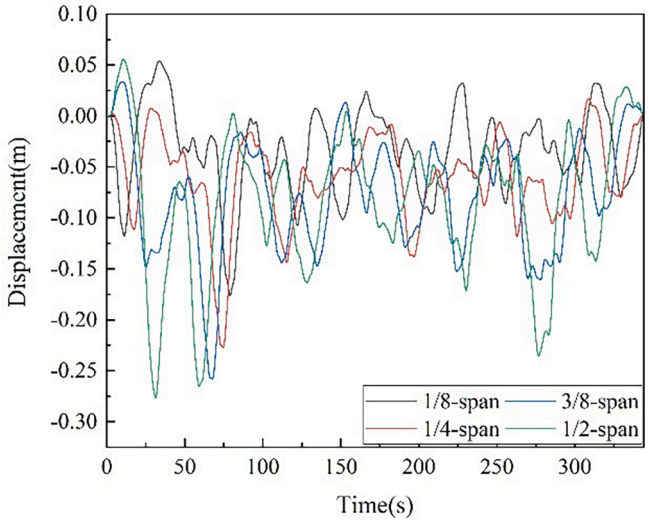

Fig. 11. The displacement time histories along the Runyang suspension bridge in Case2.

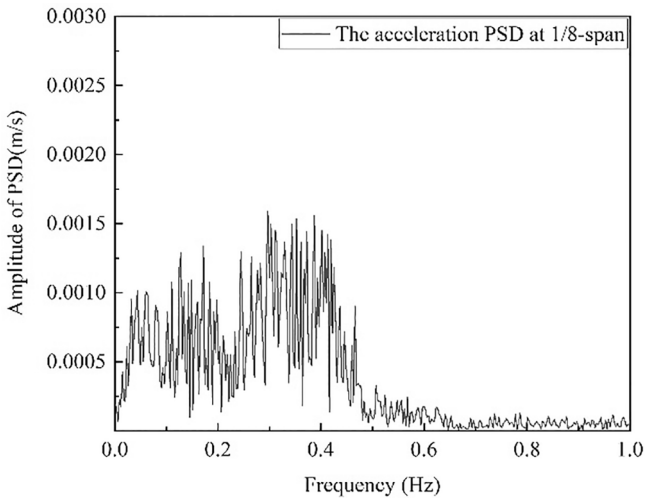

Fig. 12. The PSD of acceleration time history within 0 Hz to 1 Hz at 1/8-span.

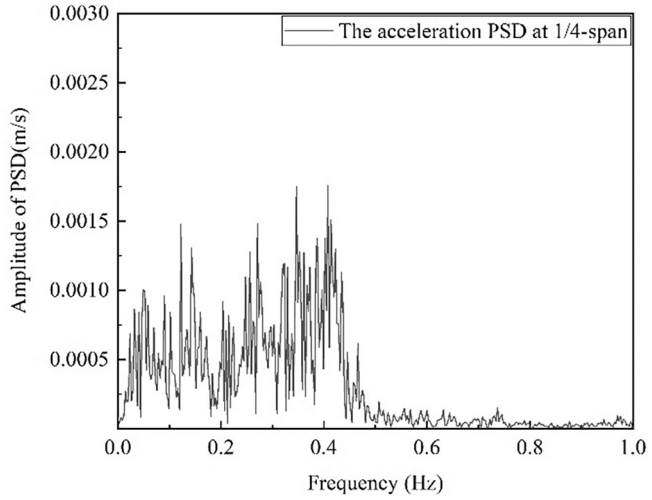

Fig. 13. The PSD of acceleration time history 0 Hz to 1 Hz at 1/4-span.

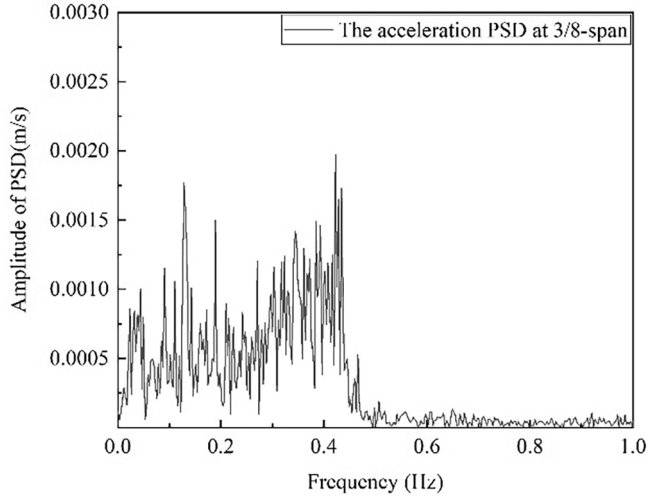

Fig. 14. The PSD of acceleration time history 0 Hz to 1 Hz at 3/8-span.

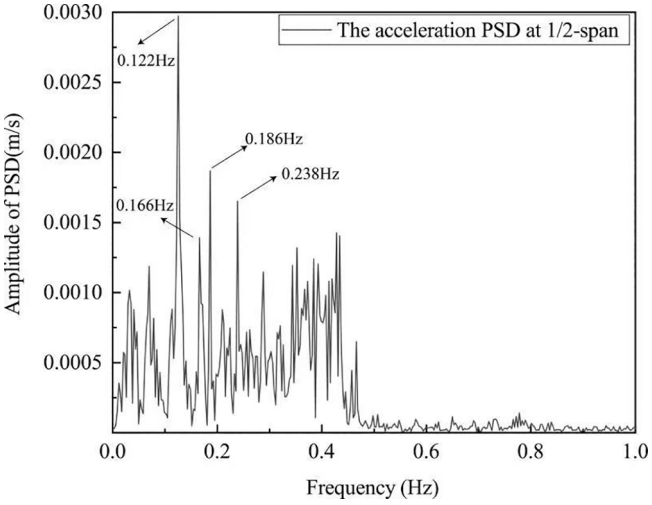

Fig. 15. The PSD of acceleration time history 0 Hz to 1 Hz at 1/2-span.

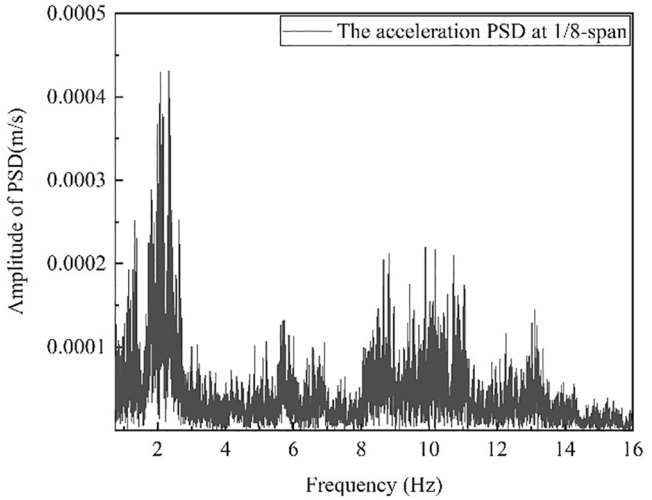

Fig. 16. The PSD of acceleration time history within 1.5 Hz to 16 Hz at 1/8-span.

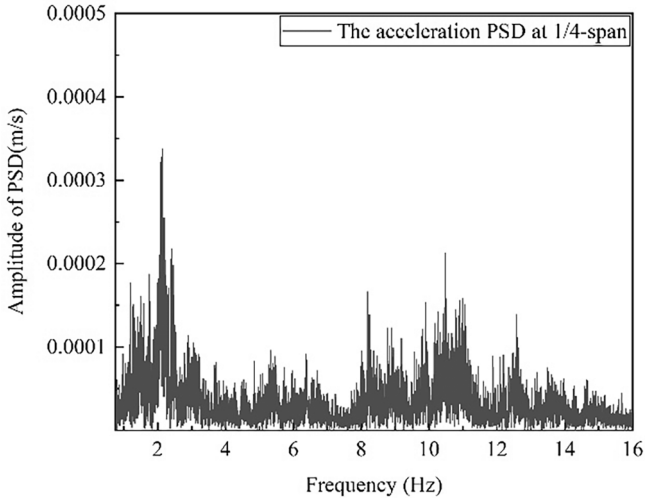

Fig. 17. The PSD of acceleration time history within 1.5 Hz to 16 Hz at 1/4-span.

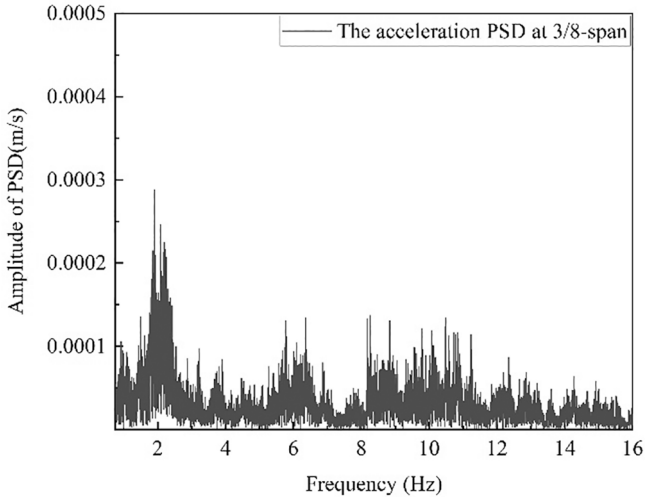

Fig. 18. The PSD of acceleration time history within 1.5 Hz to 16 Hz at 3/8-span.

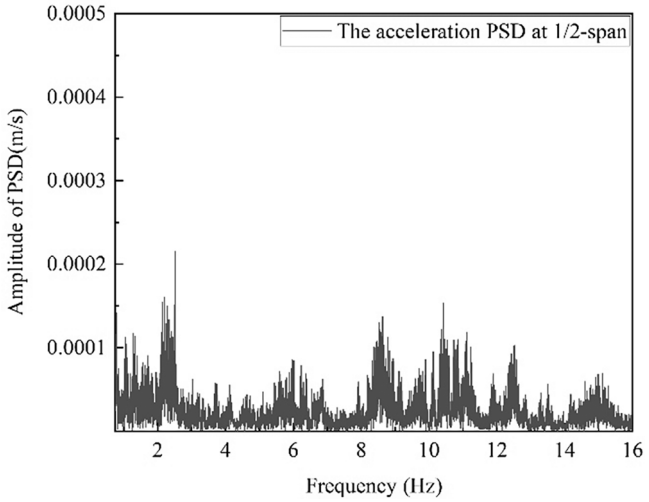

Fig. 19. The PSD of acceleration time history within 1.5 Hz to 16 Hz at 1/2-span.

6. Conclusion

This study presents a methodology to numerically simulate the VBI process for a long-span suspension bridge under the action of random traffic load in the linear range. The simulation was based on the precise time-integration linear VBI method [35], and the road surface roughness was in consideration. In random traffic flow design, traffic volume was obtained by the statistical traffic data from highway tolls station. The vehicles' sequence and gaps were sampled based on the traffic distribution surveys. According to the characteristics of traffic flow in a day, three typical loading cases was applied in the VBI dynamic response analysis. From the simulation process and numerical analysis performed, the following conclusions can be drawn:

1) To realize multi-lane loading of traffic flow, SHELL63, BEAM4, and LINK10 elements was applied in the finite element modeling of Runyang suspension bridge to consider the main girder, bridge towers, cables, and suspenders respectively. The modal analysis results showed that the bridge model and the actual bridge were well matched.
2) Comparing the max acceleration between simulation results and SHM data, the maximum acceleration obtained from SHM data was slightly larger than that simulated in VBI system at different bridge locations. However, the variation trend of maximum acceleration from 1/8-span to 1/2 span of bridge was similar.
3) The VBI analysis of displacement response indicated that the displacement response of Runyang suspension bridge was most sensitive to the traffic volume of heavy vehicles, such as M4 and M5 type vehicles, rather than other influence factor such as total volume of traffic. 1/2-span of the bridge was the location where the maximum displacement occurred. 3/8-span of bridge was another vulnerable location when heavy vehicles crossed the bridge, as the maximum displacement at this location reached 92 % of the maximum displacement at 1/2-span in Case2. The maximum displacement at 1/4-span of the bridge showed a high sensitivity both to the total volume traffic flow and the volume of heavy vehicles.
4) In the analysis of bridge's natural frequencies, the modes frequencies of VS1, VS2, VA2, VS3 could be clearly identified from the amplitude peak in the acceleration PSD distribution at 1/2-span of bridge. In the vehicle induced forced vibration analysis, the influence of vehicle body-bounce excited forced vibration was decreases gradually from 1/8-span to 1/2-span of the bridge.

Declaration of Competing Interest

The authors declare that they have no known competing financial interests or personal relationships that could have appeared to influence the work reported in this paper.

Acknowledgment

This paper was supported by National Natural Science Foundation of China (Grant Number 52178119, 51778135), the Distinguished Young Scientists of Jiangsu Province (Grant. BK20190013).

References

[1] Montenegro PA, Castro JM, Calçada R, Soares JM, Coelho H, Pacheco P. Probabilistic numerical evaluation of dynamic load allowance factors in steel modular bridges using a vehicle-bridge interaction model[J]. Eng Struct 2021;226:111316.
[2] Green M, Cebon D. Dynamic response of highway bridges to heavy vehicle loads: theory and experimental validation[J]. J Sound Vib 1994;170(1):51–78.
[3] Henchi K, Fafard M, Talbot M, Dhatt G. An efficient algorithm for dynamic analysis of bridges under moving vehicles using a coupled modal and physical components approach[J]. J Sound Vib 1998;212(4):663–83.
[4] Kim CW, Kawatani M, Kim KB. Three-dimensional dynamic analysis for bridge–vehicle interaction with roadway roughness[J]. Comput Struct 2005;83(19–20):1627–45.
[5] Law S, Zhu X. Bridge dynamic responses due to road surface roughness and braking of vehicle[J]. J Sound Vib 2005;282(3–5):805–30.
[6] An L, Li D, Yu P, Yuan P. Numerical analysis of dynamic response of vehicle–bridge coupled system on long-span continuous girder bridge[J]. Theor Appl Mech Lett 2016;6(4):186–94.
[7] Zhu X, Law S. Dynamic load on continuous multi-lane bridge deck from moving vehicles[J]. J Sound Vib 2002;251(4):697–716.
[8] Zhou J, Chen Z, Yi J, Ma H. Investigation of multi-lane factor models for bridge traffic load effects using multiple lane traffic data[J]. Structures 2020;24:444–55.
[9] Zhou J, Shi X, Ruan X, et al. Lane load disparities and their loading effect characteristics of freeway[J]. Journal of Tongji University (Natural Science) 2018;46(4):458–64.
[10] Zou Q, Deng Lu, Guo T, Yin X. Comparative study of different numerical models for vehicle–bridge interaction analysis[J]. Int J Struct Stab Dyn 2016;16(09):1550057.
[11] Kwasniewski L, Li H, Wekezer J, Malachowski J. Finite element analysis of vehicle–bridge interaction[J]. Finite Elem Anal Des 2006;42(11):950–9.
[12] Miguel LFF, Lopez RH, Torii AJ, Miguel LFF, Beck AT. Robust design optimization of TMDs in vehicle–bridge coupled vibration problems[J]. Eng Struct 2016;126:703–11.
[13] Deng Lu, Cao R, Wang W, Yin X. A multi-point tire model for studying bridge–vehicle coupled vibration[J]. Int J Struct Stab Dyn 2016;16(08):1550047.
[14] Lou P. A vehicle-track-bridge interaction element considering vehicle's pitching effect[J]. Finite Elem Anal Des 2005;41(4):397–427.
[15] Han Y, Li K, He X, Chen S, Xue F. Stress analysis of a long-span steel-truss suspension bridge under combined action of random traffic and wind loads[J]. J Aerosp Eng 2018;31(3).
[16] Li Y, Ma X, Zhang W, et al. Updating time-variant dimension for complex traffic flows in analysis of vehicle–bridge dynamic interaction[J]. J Aerosp Eng 2018;31(4):04018041.
[17] Stoura CD, Paraskevopoulos E, Dimitrakopoulos EG, Natsiavas S. A dynamic partitioning method to solve the vehicle-bridge interaction problem[J]. Comput Struct 2021;251:106547.
[18] Guo F, Cai H, Li H, Pekař L. Impact Coefficient Analysis of Curved Box Girder Bridge Based on Vehicle-Bridge Coupling[J]. Mathematical Problems in Engineering 2022;2022:1–11.
[19] Yang JP. Theoretical formulation of three-mass vehicle model for vehicle–bridge interaction[J]. Int J Struct Stab Dyn 2021;21(07):2171004.
[20] Shao Y, Brownjohn JMW, Miao C, Wang M. A precise time-integration linear vehicle-bridge interaction method and dynamic sensitivity analysis[J]. Structures 2021;33:4596–603.
[21] Jtg. D60: General specifications for design of highway bridges and culverts.[S]. China Communications Press Co, Ltd 2015. in Chinese.
[22] Li S, Yu L, Tian B, et al. Research on axle-wheel type and geometric parameters of heavy load vehicle in China[J]. Highway 2011;7:1–7.
[23] Lin S, Huang Q, Ren Y, et al. Traffic load model based on the third Nanjing Yangtze river bridge[J]. Journal of Southeast University (Natural Science Edition), 2016 (2016, 02): 365-370 (in Chinese).
[24] JT/T 489-2003: Vehicle classification of the toll for high way[S]. 2003 (in Chinese).
[25] Li W, Xia Z, Zong Z. Analysis of vehicle load model of highway bridge[J]. HIGHWAY 2010;7:14–7. in Chinese.
[26] Lu D, Lin-Li D, Wei H, et al. Study on vehicle model for vehicle-bridge coupling vibration of highway bridges in China[J]. China Journal of Highway and Transport 2018;31(7):92.

[27] OBrien EJ, Cantero D, Enright B, González A. Characteristic dynamic increment for extreme traffic loading events on short and medium span highway bridges[J]. Eng Struct 2010;32(12):3827–35.
[28] JT/T H21-2011: Standard for Technical Condition Evaluation of Highway Bridge [S]. China Communications Press, 2011 (in Chinese).
[29] Zhou Z-J, Xu X-J. Transverse distribution characteristics of vehicles in different function urban road[J]. Communications Standardization 2008.
[30] Daliang GTLaZ. Multiple-peaked probabilistic vehicle load model for highway bridge reliability assessment[J]. Journal of Southeast University (Natural Science Edition) 2008.
[31] Zong Z, Li F, Xia Y, et al. Study of vehicle load models for Xinyi River Bridge based on WIM data[J]. Bridge Constr 2013;43:29–36.
[32] Zhouhong Z, Cheng X, Zegang Y, et al. Vehicle load model for highway bridges in Jiangsu province based on WIM[J]. Journal of Southeast University (Natural Science Edition), 2020 (in Chinese), 50(1): 143-152.
[33] Li Z, Feng MQ, Luo L, Feng D, Xu X. Statistical analysis of modal parameters of a suspension bridge based on Bayesian spectral density approach and SHM data[J]. Mech Syst Sig Process 2018;98:352–67.
[34] Li Z, Li A, Zhang J. Effect of boundary conditions on modal parameters of the Run Yang Suspension Bridge[J]. Smart Struct Syst 2010;6(8):905–20.
[35] Shao Y, Brownjohn JMW, Miao C, Wang M. A precise time-integration linear vehicle-bridge interaction method and dynamic sensitivity analysis[C]. Structures 2021;33:4596–603.
[36] GB/T7031-2005: Mechanical vibration - Road surface profiles - Reporting of measured data[S]. 2005 (in Chinese).
[37] Law S-S, Zhu X-Q. Moving Loads-Dynamic Analysis and Identification Techniques: Structures and Infrastructures Book Series[M]. 8. CRC Press, 2011.
[38] Liu Y. Investigation on finite element modeling of long-span suspension bridge for structural health monitoring[D]. Nanjing: Southeast University; 2005.